percent copper. To model the process, it was assumed that the transformation follows the unreacted core model with chemical control. The expected efficiency of copper removal was 98.6 percent.

Conclusions

The sulfation of molybdenite concentrates at 160 to 190 °C with pure acid (purity greater than 96 percent) is an adequate alternative to remove copper and most other contained impurities, leaving a purified concentrate with less than 0.1 weight percent copper and low levels of other metals, dissolving less than 0.5 weight percent of the molybdenite. For up to 7 weight percent copper, conditions required are temperature of 190 °C, reaction time of 14 h and molybdenite concentrate to acid weight ratio of 1/1.

The reactor's required design and construction materials are crucial to obtain the targeted level of copper in the product and to reach an effective corrosion protection of the reactor. The basic design for an 80-t/d molybdenite concentrate plant with 4 weight percent copper requires five 8-m^3 backmixed reactors in series, operating at 190 °C and with reaction time of 10 h. The reactor must be protected with either Teflon, glass or ceramic against severe corrosion. ■

Selected references

1. Prater JD, Queneau PB, Hudson TJ (1970) The sulfation of copper-iron sulfides with concentrated sulfuric acid. J Metals 22:23–27
2. Spedden HR, Prater JD, Queneau PB, Foster GG, Pickles WS (1971) Acid-bake-leach-flotation treatment of offgrade molybdenite. Metall Mater Trans B 2:3115–3122

Analysis of SLAM-based lidar data quality metrics for geotechnical underground monitoring

Lukas Fahle*, Elizabeth A. Holley, Gabriel Walton, Andrew J. Petruska and Jurgen F. Brune
Colorado School of Mines, Golden, CO, USA
*Corresponding author email: lukasfahle@mines.edu

Full-text paper:
Mining, Metallurgy & Exploration (2022) 39:1939–1960, https://doi.org/10.1007/s42461-022-00664-3

Keywords: Mobile laser scanning, Simultaneous localization and mapping (SLAM), Geotechnical monitoring, Change detection, Rockfall and convergence

Adverse ground behavior events, such as convergence and ground falls, pose critical risks to underground mine safety and productivity. Today, monitoring of such failures is primarily conducted using legacy techniques with low spatial and temporal resolution while exposing workers to hazardous environments. This study assesses the potential of novel simultaneous localization and mapping (SLAM)-based light detection and ranging (lidar) data quality for rapid, digital and, eventually, autonomous minewide underground geotechnical monitoring. We derive a comprehensive suite of quality metrics based on tests in two underground mines for two state-of-the-art mobile laser scanning (MLS) systems. Our results provide evidence that SLAM-based MLS systems provide data of the quality required to detect geotechnically relevant changes while being significantly more efficient for large mine layouts when compared to traditional static systems. Additionally, we show that SLAM-specific processing can achieve an order of magnitude better relative accuracy relevant for change detection than quality metrics derived from traditionally deployed tests would suggest, while reducing SLAM-drift error by up to 90 percent. In collaboration with an operating block-caving mine, we confirm these capabilities in field tests on a minewide scale and, for the first time, demonstrate methods of rockfall detection using MLS data. While more work is required to investigate optimal collection, processing and utilization of MLS data, we demonstrate its potential to become an effective and widely applicable data source for rapid, accurate and comprehensive geotechnical inspections.

Table 1 — Overview of target- and site-scale tests and metrics used in study.

Results section	Tested variable	Key metric
Data quality investigation	Normality	QQ-plot, skewness, kurtosis
	Density	Minimum spacing
	Coverage	Percent occlusion
	Absolute accuracy	Trueness (μ/m)
		Precision (σ/MAD)
	Relative accuracy	Trueness (μ/m)
		Precision (σ/MAD)
		Intrinsic and extrinsic SLAM precision (σ/MAD)
MLS operational tests	Data collection efficiency	Points per second
	Loop-closure quality	Delta sensor accuracy and delta x, y, z static
	SLAM-registration quality	m/MAD
	Rockfall and convergence detection	Visual comparison/practical detection limit

μ = mean error of the distribution, m = median, σ = standard deviation, MAD = median absolute deviation.

Background

SLAM-based MLS systems show promise for large-scale, multiepoch and frequent underground mine monitoring applications [1,2]. Because mobile units such as standalone MLS systems and sensor payloads on autonomous mining equipment do not need to be set up at a specific scan station, they can significantly increase lidar data collection speed. The high temporal and spatial resolution of MLS data makes it ideal for rock-mass deformation and failure monitoring applications [3]. Although research on mobile lidar systems in underground environments has been ongoing for more than 20 years [4], geotechnical monitoring of the failures described above has not been investigated in much detail.

Methods

Our study aims to provide a current and detailed analysis of MLS lidar data quality by deploying two state-of-the-art SLAM-based systems (Kartaa Stencil 2 and Emesent Hovermap) and two static lidar scanners (Faro Focus S70 and 3D X 330). We collected data in two underground mines: an operational block-caving mine (Mine-A) and the Colorado School of Mines Edgar Experimental Mine (Edgar). We derived target- and site-scale quality metrics on MLS data collection efficiency, density and coverage as well as absolute and relative accuracy metrics. Furthermore, we tested the effect of loop closure and SLAM-based registration on data accuracy. We also conducted specific geotechnical monitoring tests for rockfall and convergence detection. Table 1 summarizes the complete set of tested variables and metrics used in our study.

Table 2 — Point collection efficiency of static lidar and two MLS.

	Faro Focus S70	Stencil 2	Hovermap
Trajectory length (m)	45 (single pass)	2 × 45 (in and out)	2 × 45 (in and out)
Trajectory time (s)	900	30	33
Average speed (km/h)	0.18	10.8	9.7
Total points (M)	26.1	4	5.2
Points per second (pts/s)	29,000	133,333	156,000

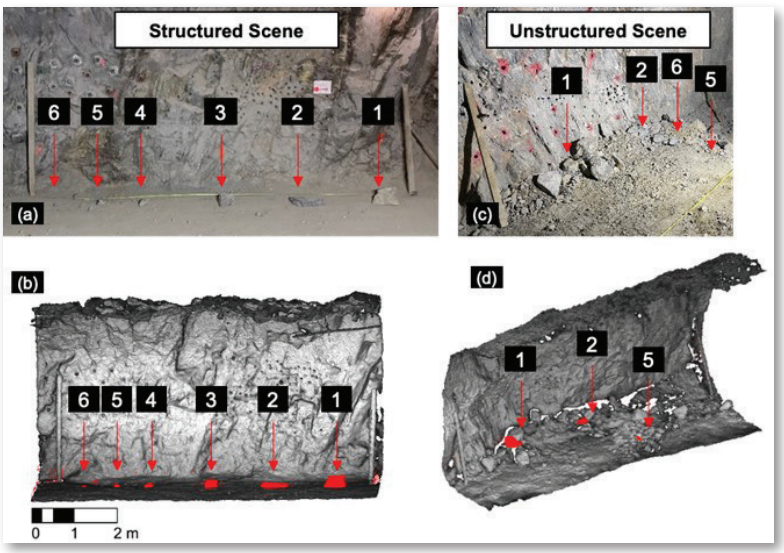

Fig. 1 Test of detectability of progressively smaller rocks, Nos. 1 (25 × 20 cm) to 6 (2.5 × 5 cm) on a flat surface in: (a),(b) structured and (c),(d) unstructured scenes with threshold filtered cloud-to-cloud distances.

Results and discussion

Efficiency. Table 2 highlights the efficiency of MLS compared to static lidar scanning. The total number of points in each of the two MLS data sets is about 80 percent lower than the number of points in the static data set. As MLS data collection is 30 times faster, the effective sampling rate measured in points per second is approximately five times higher than the rate for the static system. This is likely a lower-bound estimate, as time requirements for static scanning can increase if scans are interrupted, larger scanners and more elaborate leveling procedures are used, and the time for moving between scans is considered.

Loop closure. To evaluate the effect of SLAM-based loop closure on absolute accuracy, we registered MLS data to static data for the first 240 m of drift at Edgar by using a section, 30 m in length, at the beginning of each scan. We can observe a difference of up to 1.0 m in horizontal drift and 0.5 m in vertical drift in the nonloop-closed data. The loop-closed data shows a maximum of 0.25 m of horizontal difference and less than 5.0 cm of vertical difference from the survey data. This represents a 75 percent decrease in drift horizontal drift error and a decrease of 90 percent in vertical drift error.

Rockfall detection. Figure 1 shows two tests using Hovermap data collected at Edgar to evaluate the detectability of rock fragments in a size range typical for minor geotechnical failures that could be a potential precursor of a more significant event. In the structured scene in Figs. 1a and 1b, we can make out all six rocks with the smallest (No. 6) measuring about 2.5 × 5 cm. Four rocks from the structured scene were placed in the unstructured scene in Figs. 1c and 1d. The larger three (Nos. 1, 2, 5) can be easily detected using cloud-to-cloud (C2C), cloud-to-mesh (C2M) and multiscale model-to-model cloud (M3C2) comparisons. The smallest (No. 6) could not be identified in a C2C comparison, while the C2M and M3C2 analyses resulted in small but noticeable change signatures.

Convergence detection. Figure 2 shows an example of our mine-scale convergence monitoring tests at Mine-A. Over three months, we can detect significant changes in (A), (B) and (C) based on M3C2-distance computations and an assumed 3-cm limit of detection. Geotechnical engineers at Mine-A confirmed that changes in (A) correlate with the construction of concrete road surfaces and shotcrete work in the mine roof. The changes in (B) represent mining-induced convergence of

up to 10 cm (1.0 mm/d) in the mine roof and ribs. Visual and range-finder monitoring confirmed both the magnitude and location of the convergence.

Conclusion

Our study shows that MLS lidar data conform to or exceed the required quality to detect geotechnically relevant changes, and MLS monitoring can outperform static lidar scanning in target- and site-level coverage, uniformity of spatial sample distribution, and efficiency. In combination with advanced SLAM features like loop closure and scan registration, MLS data have the potential to become an effective and ubiquitous data source for rapid, accurate and comprehensive geotechnical inspections. More work will be required to test the sensitivity of change detection accuracy to SLAM-based alignment and the possible improvements of site-level accuracy by tightly integrating ground-control-point constraints for the SLAM algorithm. ■

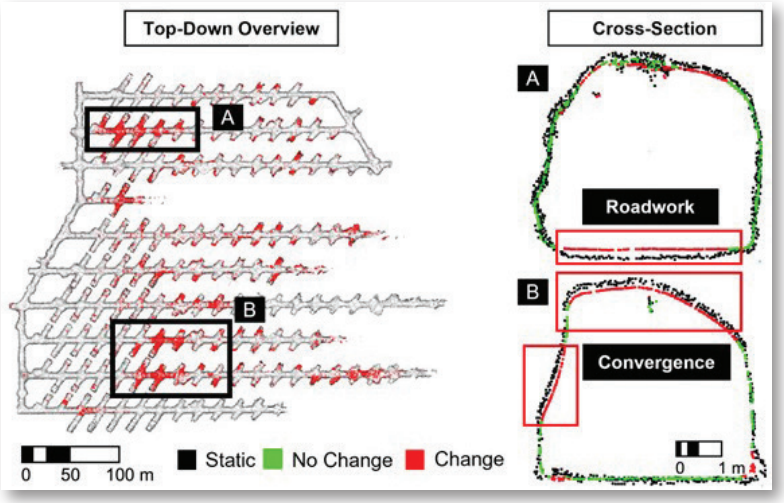

Fig. 2 Results of SLAM MLS survey at Mine-A with Stencil 2, with significant changes detected based on multiscale model-to-model cloud comparison distance calculation.

Selected references

1. Jones E, Sofonia J, Canales Cardenas C, Hrabar S, Kendoul F (2019) Advances and applications for automated drones in underground mining operations. In Proceedings of the Ninth International Conference on Deep and High Stress Mining. June 2019 pp 323–334
2. Fahle L, Holley E, Walton G (2020) Toward a mine-wide, real-time, and autonomous geotechnical change detection, monitoring, and prediction framework for underground mines. In Proceedings of the 39th International Conference on Ground Control in Mining, ICGCM, July 2020
3. Mercier-Langevin F, Hadjigeorgiou J. (2011) Towards a better understanding of squeezing potential in hard rock mines. Min Technol 120(1)36–44
4. Juneau L, Hurteau R, Freedman P, Chevrette G (1993) Using laser range data to model tunnel curvature for the automatic guidance of a mining vehicle. In Proceedings of the IEEE Conference on Control Applications 2:643–648

Collection on Ground Control in Mining

Roof stability and support strategies associated with longwall-induced horizontal stress changes in belt entries

Peter Zhang[1,*], Gabriel Esterhuizen[1], Morgan Sears[1], Jack Trackemas[1], Todd Minoski[1] and Berk Tulu[2]

[1]NIOSH, Pittsburgh Mining Research Division, Pittsburgh, PA, USA

[2]Department of Mining Engineering, West Virginia University, Morgantown, WV, USA

*Corresponding author email: nmb2@cdc.gov

Full-text paper:
Mining, Metallurgy & Exploration (2022) 39:1873–1885, https://doi.org/10.1007/s42461-022-00634-9

Keywords: Roof stability, Belt entries, Horizontal stress

Roof stability in the belt entry is critical for safe and continuous production of coal during longwall mining. Previous studies of roof falls that occurred in belt entries have shown that the roof falls were largely associated with high in situ and longwall-induced horizontal stresses [1,2,3,4]. To properly support the roof in a belt entry, it is important to understand how longwall-induced horizontal stress changes can affect roof stability in the belt entry. Monitoring of horizontal stress changes was conducted in the belt entries of two Pittsburgh seam longwall panels oriented unfavorably to the major horizontal stress. Numerical models were also set up to investigate how horizontal stress concentrates and relieves in the belt-entry roof near the face as panel orientation changes. Both measurements and modeling results show that high horizontal stress concentrates in the belt entry roof within about 15 m outby the face. The study demonstrates that longwall-induced differential horizontal stress can be used to evaluate the horizontal stress concentration factors. The horizontal stress concentration factors change with panel orientation, resulting in high stress concentrations at orientations between 20 and 110° and low stress concentrations between 130 and 180°. Roof support strategies are given for the belt entries under the influence of high horizontal stress. For unfavorably oriented panels in weak roof conditions, supplementary support should be installed during development, and cable bolts should be anchored into a stable roof horizon. The bolting pattern should be designed to cover both entry corners and the entry center to prevent potential roof cutters and sagging.